ACS APPLIED MATERIALS & INTERFACES

Research Article

www.acsami.org

# Environmentally Friendly Method: Development and Application to Carbon Aerogel as Sorbent for Solid-Phase Extraction

Sheying Dong,*[,†,‡] Guiqi Huang,[†] Meiling Su,[‡] and Tinglin Huang[†]

[†]School of Environmental and Municipal Engineering, Xi'an University of Architecture and Technology, Xi'an, Shaanxi 710055, People's Republic of China

[‡]College of Sciences, Xi'an University of Architecture and Technology, Xi'an, Shaanxi 710055, People's Republic of China

Supporting Information

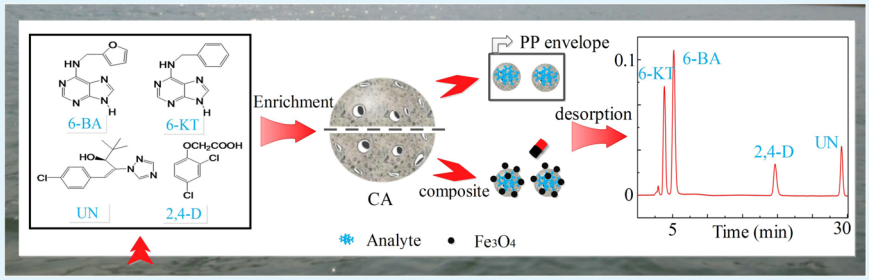


**ABSTRACT:** We developed two simple, fast, and environmentally friendly methods using carbon aerogel (CA) and magnetic CA (mCA) materials as sorbents for micro-solid-phase extraction ($\mu$-SPE) and magnetic solid-phase extraction (MSPE) techniques. The material performances such as adsorption isotherm, adsorption kinetics, and specific surface area were discussed by $N_2$ adsorption−desorption isotherm measurements, ultraviolet and visible (UV−vis) spectrophotometry, scanning electron microscopy (SEM), and high resolution transmission electron microscopy (HR-TEM). The experimental results proved that the heterogeneities of CA and mCA were well modeled with the Freundlich isotherm model, and the sorption process well followed the pseudo-second-order rate equation. Moreover, plant growth regulators (PGRs) such as kinetin (6-KT), 6-benzylaminopurine (6-BA), 2,4-dichlorophenoxyacetic acid (2,4-D), and uniconazole (UN) in a reservoir raw water sample were selected as the evaluation of applicability for the proposed $\mu$-SPE and MSPE techniques using high performance liquid chromatography (HPLC). The experimental conditions of two methods such as the amount of sorbent, extraction time, pH, salt concentration, and desorption conditions were studied. Under the optimized conditions, two extraction methods provided high recoveries (89−103%), low the limits of detection (LODs) (0.01−0.2 $\mu g\ L^{-1}$), and satisfactory analytical features in terms of precision (relative standard deviation, RSD, 1.7−5.1%, $n = 3$). This work demonstrates the feasibility and the potential of CA and mCA materials as sorbents for $\mu$-SPE and MSPE techniques. Besides, it also could serve as a basis for future development of other functional CAs in pretreatment technology and make them valuable for analysis of pollutants in environmental applications.

**KEYWORDS:** *carbon aerogel, magnetic solid-phase extraction, micro-solid-phase extraction, determination, plant growth regulators*

## 1. INTRODUCTION

In recent years, carbon aerogel (CA), as a kind of new carbon-based three-dimension nanomaterial, has obtained much attention in a variety of fields.[1−3] Generally, CA has been applied in areas like catalyst supports,[4,5] hydrogen storage,[6] an amperometric biosensor,[7] and electrode and supercapacitors.[8−10] Besides, CA and functional CAs also could provide a new extension for developing high-performance sensors according to our previously published study.[11] In the meantime, CA with remarkably high surface area and nanoscale structure, as well as mesoporous, could emerge with powerful adsorption performance.[12] Up to now, CA has been used as absorbent for dye[13] and bisphenol A[14] removal. However, there is only limited research on the preparation of coating materials on solid-phase microextraction by CA.[15] CA and functionalized CAs as sorbent materials for sample pretreatment technology have not received sufficient attention. Thus, it is anticipated that the CA and magnetic CA (mCA) solid-phase extraction (SPE) technology for monitoring and analyzing a variety of trace contaminants in the environment will have a potential study value.

SPE is a universally used separation technique for enrichment of target analytes.[16] In the past years, several kinds of SPE packing columns including ion-exchange resin,[17] silica gel,[18] and C8 and C18,[19] have been successfully applied in extracting analytes from environmental samples, but they have several drawbacks such as nonresistance to high temperature, low recovery, and selectivity, which limit extensive applications. Besides, SPE techniques require that the samples completely pass through cartridges filled with sorbents, followed by eluting

Received: June 12, 2015
Accepted: September 21, 2015
Published: September 21, 2015




DOI: 10.1021/acsami.5b05241
ACS Appl. Mater. Interfaces 2015, 7, 22256−22263

the analytes with a large number of organic solvents. This method is time-consuming, relatively expensive, and labor intensive, especially for large volumes of samples, and the sorbent packed SPE column exhibits high backpressure, which makes it difficult to adopt high flow rates. When the disperse batch mode is used, the sorbents are difficult to be separated and reused. Basheer et al. studied a new separation method named micro-solid-phase extraction ($\mu$-SPE), based on the packed sorbent materials in a porous membrane sheet which afforded protection of the sorbents.[20] The $\mu$-SPE simplified the extraction procedure, involving a single step, and no further cleanup of the extract was required. It was demonstrated to be shorter to operate, inexpensive, and a low sorbents and solvent consumption pretreatment technique. At present, some materials have been applied in the $\mu$-SPE technique for extracting organic pollutants such as carbon nanotubes (CNTs),[20] grapheme,[21] Zeolite imidazolate framework 8 (ZIF-8),[22] and $TiO_2$ nanotube.[23] These research results proved that porous materials are suitable for the $\mu$-SPE technique, and therefore, porous materials for the $\mu$-SPE technique are of great importance.

In addition, magnetic SPE (MSPE) is another novel pattern of SPE based on using a magnetic sorbent, which can be easily gathered up by means of an external magnet, greatly simplifying the phase separation process.[24] In the MSPE procedure, magnetic sorbent is an essential core, which determines the extraction efficiencies of analytes and the enrichment capability. Thus, some efforts have been made in recent years to develop various magnetic adsorbents and further to exploit their potential. For example, magnetic metal–organic frameworks[25] and multiwalled carbon nanotubes (MCNTs)[26] have been used for extracting organic pollutants (polycyclic aromatic hydrocarbons, PAHs) in various water samples. The above-mentioned two extraction techniques are proposed as the efficient, rapid, and environmentally friendly procedures for sample pretreatment, which enable the extraction of large volume samples in a short time and limit the organic solvents consumption.

Plant growth regulators (PGRs), a kind of physiological and biological compound whose effects were equivalent to endogenous counterparts, were considered as the model analytes. Some of them such as kinetin (6-KT), 6-benzylaminopurine (6-BA), 2,4-dichlorophenoxyacetic acid (2,4-D), and uniconazole (UN) (Figure 1) may be detected in water since they are widely used to improve crop and fruit production.

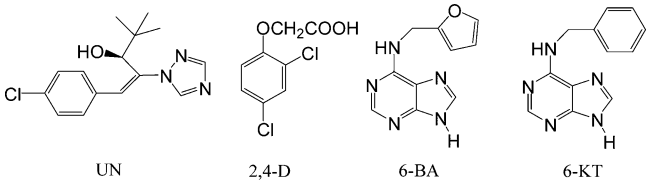


**Figure 1.** Chemical structures of four PGRs.

Herein, we present two simple, fast methods using CA and magnetic CA (mCA) materials as sorbents for $\mu$-SPE and MSPE techniques, respectively. Characterizations, adsorption, and enrichment performances of the materials were reported along with scanning electron microscopy (SEM) and high resolution transmission electron microscopy (HR-TEM), $N_2$ adsorption–desorption isotherm measurements, ultraviolet and visible (UV–vis) spectrophotometry, and high performance liquid chromatography (HPLC). As expected, CA and mCA for $\mu$-SPE and MSPE provide facile, efficient, and environmentally friendly sample preparation methods, which enable the treatment of large volume samples in a short period of time. It is worth noting that CA and mCA materials in SPE are scarce. Thus, these materials have an excellent potential research value in pretreatment technology.

## 2. EXPERIMENTAL SECTION

Apparatus, reagents, samples, and HPLC analysis were described in the Supporting Information. In addition, adsorption isotherm and adsorption kinetics also were studied according to Wei et al. reported with minor modifications.[27] (The detailed description was in Supporting Information.)

**2.1. $\mu$-SPE Procedure.** The preparation of the $\mu$-SPE device is described in the Supporting Information, and the schematic procedure of the $\mu$-SPE is shown in Figure 2. The experiments were performed according to Basheer et al.;[20] the $\mu$-SPE device was placed in a 10 mL sample solution that was stirred at 1000 rpm. After 10 min of extraction, the device was removed, dried with lint free tissue paper, and placed in a vial. The analytes were desorbed by an ultrasonic water bath with 200 $\mu$L of methanol for 10 min. Finally, the solution was filtered and used for HPLC analysis.

**2.2. MSPE Procedure.** The schematic procedure of the MSPE is also shown in Figure 2. 30 mg of mCA was added to a 10.0 mL water sample in a 25.0 mL beaker. The mixture was gently shaken for several seconds and then immersed into an ultrasonic water bath for 15 min. The sorbent was collected by applying a magnet to the beaker bottom and eluted with 200 $\mu$L of methanol in an ultrasonic water bath for 10.0 min. Finally, the solution was filtered and used for HPLC analysis.

## 3. RESULTS AND DISCUSSION

**3.1. Preparation of CA and mCA.** CA was prepared by a microwave assisted heating method according to our previous work,[11] which was described in the Supporting Information. More importantly, the alkaline catalyst is very useful in order to obtain low-density as well as high-surface area CA materials at ambient pressure drying conditions, which is necessary for the subsequent cross-linking reaction of RF aerogel, and will affect the size and stacking of the organic particles as well as thus improve the strength of aerogel network. It was worth mentioning that anhydrous sodium carbonate ($Na_2CO_3$), sodium dodecyl sulfate (SDS), and hexamethylenetetramine (HMTA) affected the speed of color change in the reaction process, which implied that the catalytic activity of polycondensation of resorcinol with formaldehyde can be estimated. The fastest aerogel reaction speed was anhydrous $Na_2CO_3$ as catalyst, followed by HMTA; the slowest was SDS. As a result, their catalytic activity order was: anhydrous $Na_2CO_3$ > HMTA > SDS; finally, we chose the anhydrous $Na_2CO_3$ as the catalyst in the process of synthesis CA. Meanwhile, it was observed that the skeletal structure of the CA using the microwave assisted method consisted of interconnected nanosized carbon ligaments that defined a continuous polyporous network and had no obvious difference with the conventional method.[28]

As far as we know, for the fabrication of nanosized $Fe_3O_4$ doped CA that is mCA, none of the published studies were reported by the chemical precipitation method[29] (for details, see the Supporting Information). The precipitant $NH_3{\cdot}H_2O$ was adopted during the reaction between $Fe^{2+}$ and $Fe^{3+}$ in this study to keep crystal nucleation growth.[30] Besides, the pH also affected the size of the $Fe_3O_4$ particles in the reaction process, which means that the surface areas of the mCA can be varied.


DOI: 10.1021/acsami.5b05241
ACS Appl. Mater. Interfaces 2015, 7, 22256–22263

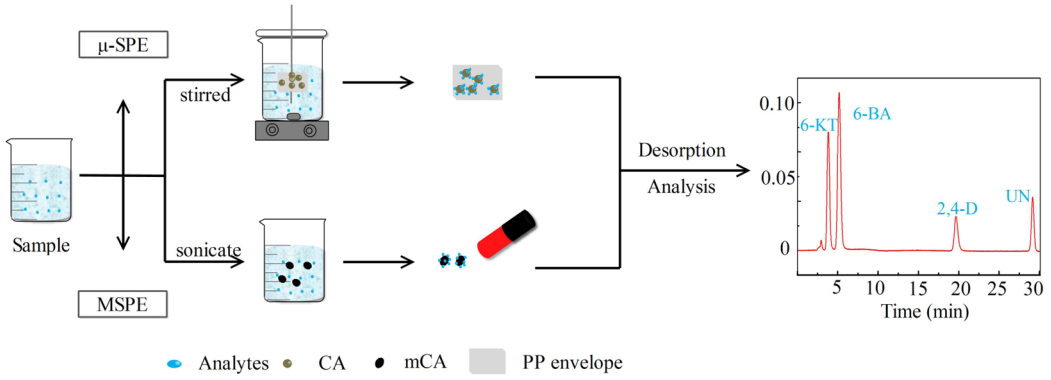


**Figure 2.** Schematic illustration of $\mu$-SPE and MSPE procedure and analysis.

In the meantime, we designed three mCA materials by changing the mass ratios of $Fe_3O_4$ and CA (1:5, 1:10, 1:20).

**3.2. Characterization and Textural Properties of CA and mCA.** Powder X-ray diffraction images of the $Fe_3O_4$ (standard card), CA, and mCA (1:10) are shown in Figure 3A. The diffraction peaks of the mCA showed that $Fe_3O_4$ and the CA crystal were well retained because all diffraction peaks of mCA (Figure 3A-3) were readily indexed to $Fe_3O_4$ (Figure 3A-1) and CA (Figure 3A-2), respectively.

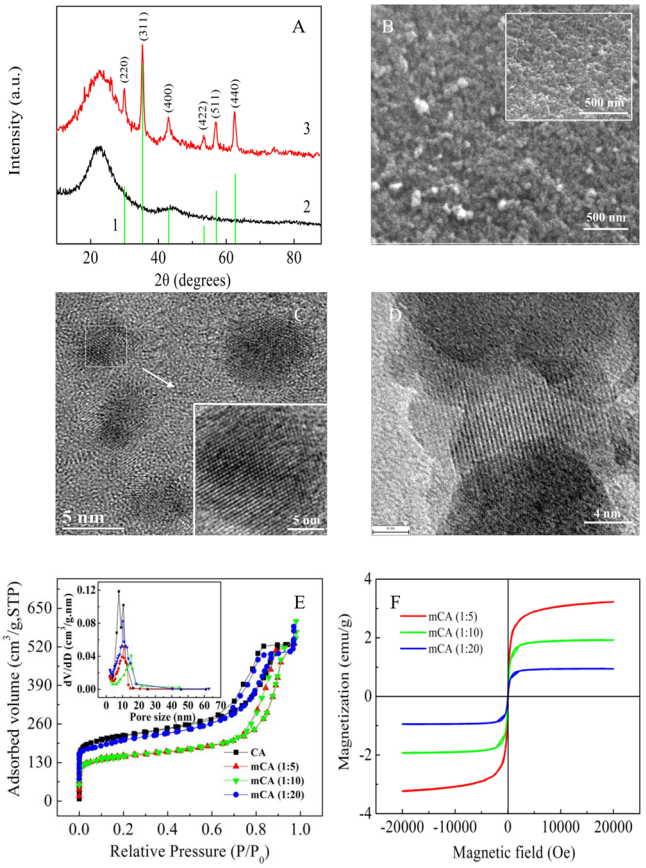


**Figure 3.** (A) XRD pattern of $Fe_3O_4$ (standard card), CA, and mCA (1:10); (B) SEM images of mCA (1:10) and CA (inset); (C, D) HR-TEM images of CA and mCA (1:10); (E) nitrogen adsorption–desorption isotherms and pore size distribution curves (inset) of CA and three mCA materials; (F) magnetization curves of three mCA materials.

The surface characteristics of CA and mCA were investigated by scanning electron microscopy (SEM). Figure 3B is a micrograph of mCA (1:10) and CA (Figure 3B inset), respectively. Detailed views clearly revealed that lots of pores and channels appeared on the surface of both CA and mCA materials. Because the CA was not completely covered by the $Fe_3O_4$ nanoparticles ($Fe_3O_4$ NPs), the composite was expected to have the adsorption properties of CA and exhibits the good ferromagnetic property of $Fe_3O_4$ NPs, which was sufficient for magnetic separation with a conventional magnet. Figure 3C,D showed the HR-TEM images of CA and mCA (1:10). In the HR-TEM images, the graphite phase morphology of CA and mCA was clearly observed, indicating the formation of the interconnected microstructure. On the other hand, the HR-TEM image of mCA (Figure 3D) also provides evidence for $Fe_3O_4$ NPs being decorated onto the CA phase matrix, implying that mCA is formed and its morphology is unchanged.

Nitrogen sorption was performed to study the pore properties of the CA and mCA materials. As displayed in Figure 3E, the $N_2$ adsorption–desorption isotherms of the CA and mCA exhibit a type-IV curve with small hysteresis, which indicates some interstitial structures form among the aggregated particles in the samples. Simultaneously, the CA and mCA materials showed a narrow pore size distribution (see the Figure 3E inset); the phenomenon can be explained in our previous study.[11] Besides, as can be seen from Figure 3A and Table 1, the surface areas of CA and three kinds of mCA

**Table 1. BET Surface Area, Pore Diameter, and Volume of CA and Three mCA Materials**

| samples | BET surface area ($m^2$/g) | average pore diameter (nm) | pore volume ($cm^3$/g) |
|---|---|---|---|
| CA | 747 | 7.9 | 0.61 |
| mCA (1:5) | 510 | 10.2 | 1.18 |
| mCA (1:10) | 523 | 16.4 | 2.06 |
| mCA (1:20) | 675 | 10.1 | 0.73 |

materials are in the order CA > mCA (1:20) > mCA (1:10) > mCA (1:5). The textural properties of CA still were unchanged in three mCA materials despite the Brunauer–Emmett–Teller (BET) surface area of the three mCA materials slightly decreased.

Figure 3F showed the magnetic hysteresis loops of three mCA materials. This feature illustrated that three mCA materials responded magnetically to an external magnetic


DOI: 10.1021/acsami.5b05241
ACS Appl. Mater. Interfaces 2015, 7, 22256–22263

field, and this response vanished upon the removal of the magnetic field. The saturation magnetization of three mCA materials was 3.23, 1.93, and 0.94 emu $g^{-1}$, respectively. Three mCA materials kept enough of a magnetic response to meet the need of magnetic separation.

**3.3. Adsorption Performance of CA and mCA.** The adsorption isotherms of UN on CA and mCA were investigated at 25 °C (as shown in Figure 4A). The adsorption capacities

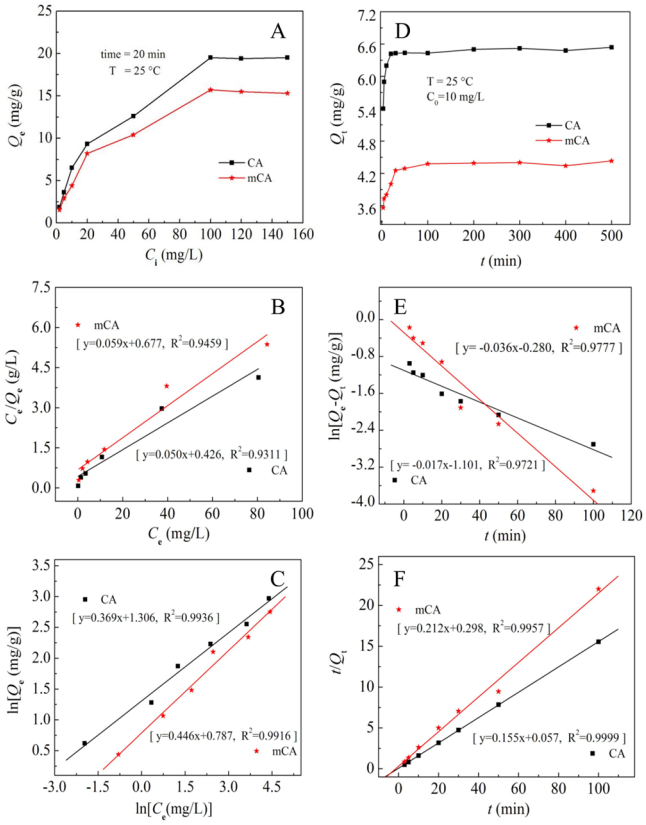


**Figure 4.** Left: (A) Adsorption isotherm curves; (B) Langmuir isotherm models; (C) Freundlich isotherm models. Right: (D) Adsorption amount−time curves; (E) pseudo-first order sorption kinetics; (F) pseudo-second order sorption kinetics of UN on CA and mCA.

($Q_0$) of CA and mCA for UN increased along with the increase of UN concentration, and the $Q_{max,0}$ of CA and mCA for UN from aqueous solutions achieved about 20 and 16 mg $g^{-1}$, respectively. Meanwhile, the $Q_0$ for CA was greater than that of mCA at the identical UN concentration; it may be ascribed to CA providing a higher-affinity for UN than mCA, which was consistent with the results of nitrogen adsorption−desorption isotherms. In addition, some performance data of the previous reports materials, CA and mCA, were also discussed in the Supporting Information.

The equilibrium data were modeled with the Langmuir equation and the Freundlich equation according to Wei et al.[27] Figure 4B,C shows the isotherm equation and the correlation coefficient ($R^2$) for UN adsorbed on CA and mCA. The Freundlich isotherm model matched the experimental data better since it had a higher correlation coefficient than the Langmuir isotherm model. On the basis of the higher $R^2$ value of the Freundlich isotherm, the adsorption process described here was most likely dominated by multiple adsorptions, which may be attributed to adsorption site heterogeneity and adsorbate interactions. In addition, the value of $n$ was calculated to be 2.71 and 2.24 by using the Freundlich theory, respectively, indicating that the adsorption of CA and mCA for UN is favorable.

The adsorption amount−time curves of UN on CA and mCA were shown in Figure 4D. The absorption capacity of CA for UN increased with adsorption time, and the adsorption process was very quick for the CA whose adsorption equilibrium can be achieved within 15 min. However, it cannot reach equilibrium in more than 15 min for mCA. From the result of Table 1, the surface areas of mCA were less than those of CA, which resulted in slower adsorption. In order to determine the rate-controlling and mass transfer mechanisms, kinetic data were correlated to linear forms of the first-order equation and the second-order equation. The result shows that the $R^2$ value of the second-order adsorption model exhibited a higher value than that of the first-order model (Figure 4E,F). The high $R^2$ value of the correlation coefficient is clear evidence that the sorption process follows the pseudo-second-order rate equation. This result indicated that sorption processes are usually characterized by three consecutive steps, namely, the external diffusion, internal diffusion, and the adsorption stage according to Wei et al.[27]

**3.4. Optimization of μ-SPE and MSPE Extraction Conditions.** To obtain high extraction efficiency (EE) and relative recovery (RR), several key parameters in two procedures, including the amount of sorbent, extraction time, pH, salt concentration, and desorption conditions, were carefully studied (100 μg $L^{-1}$ of the mixed standard solution, $n$ = 3).

The extraction efficiency (EE) of the target analyte was calculated as follows:

$$\mathrm{EE}(\%) = C_1V_1/C_0V_{\mathrm{sample}} \times 100\% \quad (1)$$

where $C_1$ and $C_0$ represent the concentration of analyte in sorbents and initial concentration of the analyte in the sample solution and $V_1$ and $V_{\mathrm{sample}}$ are volumes of desorption solution and samples, respectively.

Relative recoveries (RR) of analyte were calculated as follows:

$$\mathrm{RR}\% = C_{\mathrm{found}} - C_{\mathrm{real}}/C_{\mathrm{added}} \times 100\% \quad (2)$$

where $C_{\mathrm{found}}$, $C_{\mathrm{real}}$, and $C_{\mathrm{added}}$ are the total concentration of analyte after addition of a known amount of standard in real sample, the original concentration of analyte in real sample, and the concentration of known amount of standard that was spiked in the real sample, respectively.

*3.4.1. Effect of the Composition Ratio of mCA in MSPE.* Due to their different surface areas and pore volumes, these mCAs afford different adsorption capacities for the target analytes. Therefore, different composition ratios between $Fe_3O_4$ and CA (1:5, 1:10, and 1:20) have been investigated in the experiments. The result in Figure 5 shows that the EEs of the target analytes reached the maxima when the composition ratio of mCA was 1:10. This phenomenon can be ascribed to the fact that too large of a $Fe_3O_4$ proportion reduces the surface area of mCA materials, limiting its extractability. On the contrary, when too small of a $Fe_3O_4$ proportion was used, the sorbent was difficult to be gathered by a magnet, leading to loss of a partial amount of the target analytes. Thus, 1:10 was selected as the composition ratio of mCA in MSPE.


DOI: 10.1021/acsami.5b05241
ACS Appl. Mater. Interfaces 2015, 7, 22256−22263

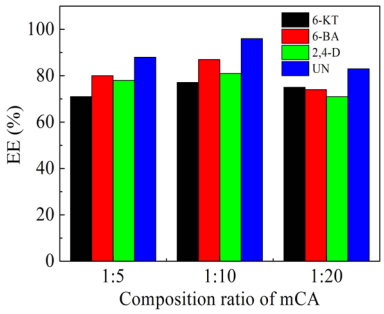


**Figure 5.** MSPE extraction conditions: the effect of the composition ratio of mCA on the EEs with the 100 $\mu$g $L^{-1}$ concentration of each PGR.

*3.4.2. Effect of the Amount of Sorbent and Extraction Time.* The amount of sorbent is an important factor in affecting EE and extraction time,[31,32] and the sorbent amount of 10−60 mg was considered for this purpose. As shown in Figure 6A,A′,

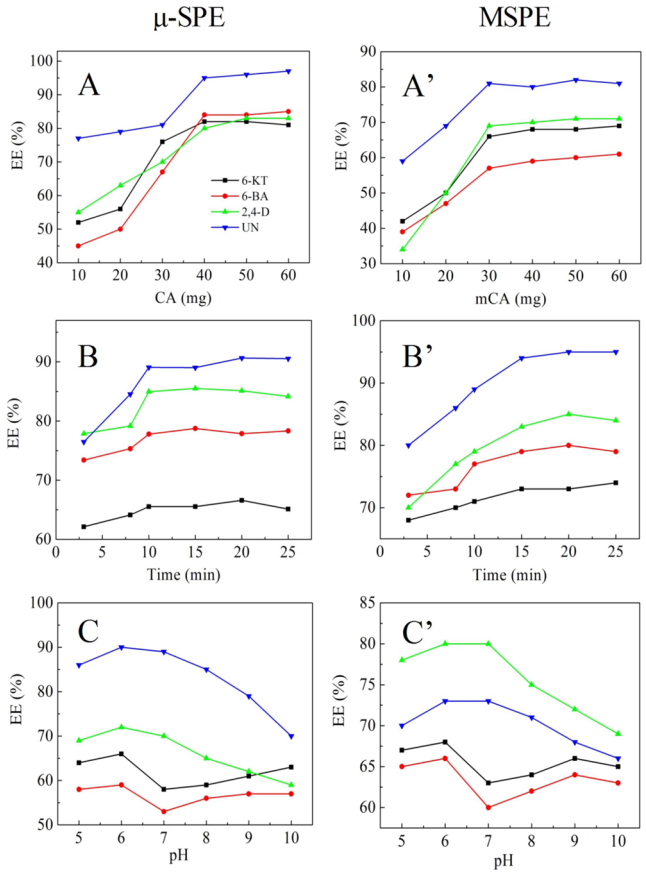


**Figure 6.** Effect of all kinds of parameters on the EEs. Extraction conditions: 100 $\mu$g $L^{-1}$ of each PGR spiked solution. Top: Effect of the amount of sorbent on (A) $\mu$-SPE and (A′) MSPE. Middle: Effect of extraction time on (B) $\mu$-SPE and (B′) MSPE. Bottom: Effect of pH value on (C) $\mu$-SPE and (C′) MSPE.

the EEs of the target analytes increased with increasing the amounts of sorbent and reached the maxima at 40 mg for $\mu$-SPE and 30 mg for MSPE. This is mainly because the target analyte of sample solution can be adsorbed on the surface of CA by entering the polypropylene (PP) sheet membrane, which is equivalent to the surface area of sorbents slightly decreasing, requiring more sorbent to reach equilibrium in the $\mu$-SPE than that in the MSPE. Besides, a further increase in sorbent amount results in little change in the EEs. These reasons can be due to the following: The sorption of the target analytes was incomplete when the small amounts of sorbents were used as extraction. In contrast, the target analytes were completely adsorbed on the CA and mCA when the amounts of sorbents increased a certain value. In order to certify the explanation above, we examined the HPLC chromatogram of the target analytes from the discarded sample solution after the adsorption. Using the sorbent (CA and mCA) to once again extract the discarded sample solution according to the method above, Sections 3.3 and 3.4, it was observed that no target analytes were detected in the discarded sample solution. Considering the dimensions of the $\mu$-SPE device and the volume of the desorption solvent, 40 mg of CA and 30 mg of mCA were finally chosen to be the optimal amount for the $\mu$-SPE and MSPE method, respectively.

The effect of extraction time on the EEs of the target analytes was evaluated. The results in Figure 6B,B′ showed that each target analyte quickly reached equilibrium. Such a fast adsorption rate could be attributed to the Freundlich theory. The adsorption of CA for analytes was favorable. However, the EEs of some target analytes decreased slightly over prolonged extraction, and similar phenomena have been reported in the literature.[33] In similar circumstances, the MSPE method achieved the highest EEs in 15 min (Figure 6B′). On the basis of these results, 10 min of extraction time was used for the $\mu$-SPE method and 15 min for MSPE, respectively.

*3.4.3. Effect of pH.* The pH value is a key factor in the extraction process because it affects the existing form of the target analytes.[34] The pH values of the sample solution ranging from 5 to 10 were tested (shown in Figure 6C,C′); when the pH value was increased, the EEs were enhanced and then decreased (At pH value in 5−7). At a pH value higher than 7, the EEs of 2,4-D and UN were decreased, but the EEs of 6-KT and 6-BA were enhanced with the increase of pH value. This may be associated with three factors: (1) UN has geometrical isomerism and optical isomerism because it contains a double bond and chiral carbon atoms in its molecular structure. It can exist stably as the form of molecules in the acidic and neutral conditions, but the double bond of uniconazole fractured under alkaline conditions. (2) 6-BA and 6-KT have a good solubility in acid and alkali media, while 2,4-D was in the anionic form in alkaline solutions. (3) The pH values were more than the isoelectric point (IEP, 6.4−6.8) of $Fe_3O_4$ NPs, and the negative charge on the $Fe_3O_4$ NPs of the mCA surface became strong, which made mutual repulsion between $Fe_3O_4$ NPs of mCA and the anionic form of 2,4-D. Thus, in the following experiments, the pH value was adjusted to 6.

*3.4.4. Salt Concentration.* To study the influence of salt addition, a variable amount of NaCl (0%, 5%, 10%, 15%, 20%, and 30% (w/v)) was added to the sample solutions while other experimental conditions were kept constant. For $\mu$-SPE and MSPE, the EEs of the target analytes were increased owing to solution solubility decreasing with increasing NaCl concentration.[22] As can be seen in Figure S1, the EEs of the target analytes increased along with the increase of NaCl concentration from 0% to 15% and then decreased when the NaCl concentration further increased. This is the salting-out effect which enhanced the EEs of the target analytes according to the previous study.[22,35] In contrast, the EEs of the target analytes decreased with the increase of NaCl concentration from 15% to 30%; this is because the mass transfer from aqueous phase to


DOI: 10.1021/acsami.5b05241
ACS Appl. Mater. Interfaces 2015, 7, 22256−22263

the sorbent was inhibited: a common observation that has been reported in previous literature.[20,21] Therefore, 15% NaCl was considered optimal in μ-SPE. Figure S2 shows that EE values also increased and then decreased with the increase in NaCl concentration. In consideration of these observations, 10% NaCl was adopted as being most favorable in the MSPE method.

*3.4.5. Effect of Desorption Conditions.* After extraction, the target analytes should be desorbed using desorption agent from sorbents prior to HPLC analysis. Desorption of analytes was studied using different organic solvents including methanol, acetone, acetonitrile, *n*-hexane, and acetic acid. Among the different desorption agents, the desorption ability of methanol was found to be higher than the other solvents.

The effect of the volume of methanol on EEs of the target analytes was further investigated. The volumes of methanol less than 200 μL were not enough to immerse the μ-SPE devices during the desorption process, which led to the poor precision of the determination. Thus, desorption experiments were carried out by using 200 to 350 μL of methanol. No significant change in the EEs was observed when the volume of methanol was varied. Thus, 200 μL was chosen for the subsequent experiments.

Desorption times were studied within the range of 3−25 min in μ-SPE and MSPE methods. Figures S3 and S4 showed that the EEs of the target analytes increased with increasing desorption time and then decreased rapidly. This phenomenon may be attributed to the fact that desorption was incomplete when shorter times were used as expected, and too long of a desorption time could give rise to the readsorption of the target analytes. After the first desorption, the solvents were further desorbed in order to test carryover effects. None of the target analytes were detected in the second desorption, which demonstrated that no target analytes were carried over. Consequently, desorption times of both methods were fixed at 10 min.

**3.5. Method Evaluation.** Analytical parameters of the two proposed methods are shown in Table 2. Satisfactory linearity

**Table 2. Liner Regression, RSD, and LODs of μ-SPE and MSPE**

| method | analyte | linearity (μg $L^{-1}$) | $r^2$ | RSD ($n$ = 3, %) | LODs (μg $L^{-1}$) |
|---|---|---|---|---|---|
| μ-SPE | 6-KT | 0.01−200 | 0.9981 | 5.1 | 0.05 |
| | 6-BA | 0.01−200 | 0.9992 | 4.2 | 0.02 |
| | 2,4-D | 0.01−200 | 0.9989 | 1.7 | 0.1 |
| | UN | 0.01−200 | 0.9990 | 5.0 | 0.01 |
| MSPE | 6-KT | 0.01−200 | 0.9985 | 3.3 | 0.04 |
| | 6-BA | 0.01−200 | 0.9990 | 4.0 | 0.03 |
| | 2,4-D | 0.01−200 | 0.9990 | 1.9 | 0.2 |
| | UN | 0.01−200 | 0.9983 | 2.1 | 0.01 |

of both methods was obtained with correlation coefficients above 0.9981. The limits of detection (LODs) (S/N = 3) were between 0.01 and 0.2 μg $L^{-1}$. Therefore, the μ-SPE had better extraction performance than the MSPE method. Most LODs obtained by μ-SPE and MSPE also were lower than other extraction methods except reversed-dispersive solid-phase extraction (as shown in Table 3). Nevertheless, fewer sample volumes and organic solvents were applied in the μ-SPE and MSPE than in the conventional SPE method. Additionally, the outstanding advantage of μ-SPE is the fast extraction speed.

**Table 3. Analytical Performance Data of Other Methods**

| analytes | method[a] | samples | LODs (μg $L^{-1}$) | recoveries (%) | ref |
|---|---|---|---|---|---|
| 6-KT | IL-ATPS | sediment | 0.03 | 97 | 34 |
| | IL-MAE | sediment | 0.06 | 100 | 34 |
| 6-BA | IL-ATPS | sediment | 0.06 | 98 | 34 |
| | IL-MAE | sediment | 0.12 | 118 | 34 |
| 2,4-D | SPE | water | | 90 | 36 |
| UN | USA-DLLME | soil | 50 | 89 | 37 |
| | QuEChERS | fruits | 0.006 | 80 | 38 |

[a]IL-ATPS: ionic/salt aqueous two-phase system; IL-MAE: ionic liquid-based microwave-assisted extraction; SPE: solid-phase extraction; USA-DLLME: ultrasound assisted dispersive liquid−liquid microextraction; QuEChERS: reversed-dispersive solid-phase extraction.

The probable reason is the surface areas of CA being greater than mCA. When using mCA as sorbents, compared with μ-SPE, the MSPE method has wider applicability and low price. For example, μ-SPE usually does not apply to a large number of samples in a short time, since it is necessary to prepare a lot of PP sheet membrane envelopes.

**3.6. Application for Real Sample.** To test the applicability of the two methods, the reservoir raw water sample in Shan Dong of China was analyzed ($n$ = 3). Figure 7

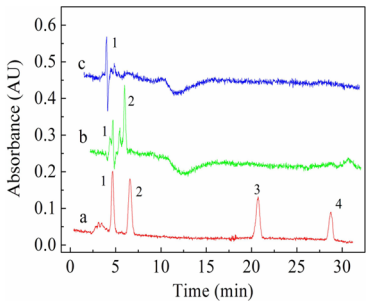


**Figure 7.** Chromatograms of analyzed samples. (a) Concentration of 100 μg $L^{-1}$ of the mixed standard solution, (b) μ-SPE, and (c) MSPE. Peak identification: 1, 6-KT; 2, 6-BA; 3, 2,4-D; 4, UN.

shows the HPLC chromatograms using the μ-SPE and MSPE methods, respectively. Results in Table 4 showed that 6-BA and 6-KT were detected with a concentration of 3.0 and 7.8 μg $L^{-1}$ by the μ-SPE method and 6-KT was detected with a

**Table 4. Determination Results and RR of PRGs in a Reservoir Raw Water Sample by μ-SPE and MSPE[a]**

| | | water sample (Shan Dong) | | | |
|---|---|---|---|---|---|
| | | nonspiked | | spiked | |
| method | analytes | concentration (μg $L^{-1}$) | RSD% ($n$ = 3) | RR (%) | RSD% ($n$ = 3) |
| μ-SPE | 6-KT | 7.8 | 3.2 | 97 | 1.7 |
| | 6-BA | 3.0 | 1.8 | 95 | 1.3 |
| | 2,4-D | nd | | 92 | 3.6 |
| | UN | nd | | 101 | 2.4 |
| MSPE | 6-KT | 6.0 | 2.6 | 91 | 4.7 |
| | 6-BA | nd | | 89 | 1.5 |
| | 2,4-D | nd | | 91 | 3.0 |
| | UN | nd | | 99 | 3.2 |

[a]nd: not detected.



DOI: 10.1021/acsami.5b05241
ACS Appl. Mater. Interfaces 2015, 7, 22256−22263

concentration of 6.0 $\mu$g $L^{-1}$ by the MSPE method. In addition, the relative recoveries (RRs) of the target analytes were measured to be above 89%. These results indicate that $\mu$-SPE is better than MSPE in real sample analysis.

## 4. CONCLUSIONS

In the current paper, CA and functional CA materials were applied as sorbents to enhance the extraction performance of $\mu$-SPE and MSPE procedures. Satisfactory LODs from 0.01 to 0.2 $\mu$g $L^{-1}$ and good relative standard deviation (RSD) values for four PGRs were achieved. Especially, the procedures were simple, quick, and consumed less organic solvent. As expected, this work opens up a new application for CA and functional CA materials as sorbents for sample preparation. Other functional CAs will further provide an excellent potential of improving extraction performance for a wider use in pretreatment technologies such as dispersive SPE, mixed hemimicelles SPE, and solid-phase microextraction.

## ■ ASSOCIATED CONTENT

### Supporting Information

The Supporting Information is available free of charge on the ACS Publications website at DOI: 10.1021/acsami.5b05241.

Additional experimental section and results and discussion (PDF)

## ■ AUTHOR INFORMATION

### Corresponding Author

*E-mail: dongsyy@126.com. Tel: (+86)-29-82201203. Fax: (+86)-29-82205332.

### Notes

The authors declare no competing financial interest.

## ■ ACKNOWLEDGMENTS

The authors appreciate the support from the National Natural Science Foundation of China (No. 21575111), the projects in the National Science & Technology (No. 2012BAC04B02), and the National Natural Science Foundation of China (No. 50830303).

## ■ REFERENCES

(1) Yang, K.; Zhu, L. Z.; Xing, B. S. Adsorption of Polycyclic Aromatic Hydrocarbons by Carbon Nanomaterials. *Environ. Sci. Technol.* **2006**, *40*, 1855−1861.

(2) Yin, L. W.; Zhang, Z. W.; Li, Z. Q.; Hao, F. B.; Li, Q.; Wang, C. X.; Fan, R. H.; Qi, Y. X. Spinel $ZnMn_2O_4$ Nanocrystal-Anchored 3D Hierarchical Carbon Aerogel Hybrids as Anode Materials for Lithium Ion Batteries. *Adv. Funct. Mater.* **2014**, *24*, 4176−4185.

(3) Zhang, Y. N.; Jin, Y. F.; Huang, X. F.; Shi, H. J.; Zhao, G. H.; Zhao, H. Y. Nanocrystalline $TiO_2$/Carbon Aerogel Electrode with High Surface Area and Enhanced Photoelectrocatalytic Oxidation Capacity. *Electrochim. Acta* **2014**, *130*, 194−199.

(4) Antonietti, M.; Fechler, N.; Fellinger, T. P. Carbon Aerogels and Monoliths: Control of Porosity and Nanoarchitecture via Sol-Gel Routes. *Chem. Mater.* **2014**, *26*, 196−210.

(5) Park, H. W.; Kim, J. K.; Hong, U. G.; Lee, Y. J.; Song, J. H.; Song, I. K. Catalytic Decomposition of 4-phenoxyphenol Over Pd/X Cs2.5 H 0.5PW 12O 40/ACA (Activated Carbon Aerogel)-$SO_3H$ (X = 10−30 wt%) Catalysts. *Appl. Catal., A* **2013**, *453*, 287−294.

(6) Moreno-Castilla, C.; Maldonado-Hódar, F. Carbon Aerogels for Catalysis Applications: An Overview. *Carbon* **2005**, *43*, 455−465.

(7) Peng, L.; Dong, S. Y.; Li, N.; Suo, G. C.; Huang, T. L. Construction of a Biocompatible System of Hemoglobin based on AuNPs-Carbon Aerogel and Ionic Liquid for Amperometric Biosensor. *Sens. Actuators, B* **2015**, *210*, 418−424.

(8) Saliger, R.; Fischer, U.; Herta, C.; Fricke, J. High Surface Area Carbon Aerogels for Supercapacitors. *J. Non-Cryst. Solids* **1998**, *225*, 81−85.

(9) Liu, R. L.; Wan, L.; Liu, S. Q.; Pan, L. X.; Wu, D. Q.; Zhao, D. Y. An Interface-Induced Co-Assembly Approach Towards Ordered Mesoporous Carbon/Graphene Aerogel for High-Performance Supercapacitors. *Adv. Funct. Mater.* **2015**, *25*, 526−533.

(10) Liu, W. W.; Li, X.; Zhu, M. H.; He, X. High-Performance All-Solid State Asymmetric Supercapacitor Based on $Co_3O_4$ Nanowires and Carbon Aerogel. *J. Power Sources* **2015**, *282*, 179−186.

(11) Dong, S. Y.; Li, N.; Suo, G. C.; Huang, T. L. Inorganic/Organic Doped Carbon Aerogels as Biosensing Materials for the Detection of Hydrogen Peroxide. *Anal. Chem.* **2013**, *85*, 11739−11746.

(12) Micheli, D.; Vricella, A.; Pastore, R.; Marchetti, M. Synthesis and Electromagnetic Characterization of Frequency Selective Radar Absorbing Materials Using Carbon Nanopowders. *Carbon* **2014**, *77*, 756−774.

(13) Wu, X. B.; Hui, K. N.; Hui, K. S.; Lee, S. K.; Zhou, W.; Chen, R.; Hwang, D. H.; Cho, Y. R.; Son, Y. G. Adsorption of Basic Yellow 87 from Aqueous Solution onto two Different Mesoporous Adsorbents. *Chem. Eng. J.* **2012**, *180*, 91−98.

(14) Hou, C. H.; Huang, S. H.; Chou, P. H.; Den, W. Removal of Bisphenol A from Aqueous Solutions by Electrochemical Polymerization on a Carbon Aerogel Electrode. *J. Taiwan Inst. Chem. Eng.* **2015**, *51*, 103−108.

(15) Zhu, F.; Guo, J. M.; Zeng, F.; Fu, R. W.; Wu, D. C.; Luan, Y. G.; Tong, Y. X.; Lu, T. B.; Ouyang, G. F. Preparation and Characterization of Porous Carbon Material-Coated Soild-Phase Microextraction Metal Fibers. *J. Chromatogr. A* **2010**, *1217*, 7848−7854.

(16) Zhang, Y.; Kuang, M.; Zhang, L. J.; Yang, P. Y.; Lu, H. J. An Accessible Protocol for Solid-Phase Extraction of N-linked Glycopeptides Through Reductive Amination by Amine-Functionalized Magnetic Nanoparticles. *Anal. Chem.* **2013**, *85*, 5535−5541.

(17) Tangen, G.; Wickstrøm, T.; Lierhagen, S.; Vogt, R.; Lund, W. Fractionation and Determination of Aluminum and Iron in Soil Water Samples Using SPE Cartridges and ICP-AES. *Environ. Sci. Technol.* **2002**, *36*, 5421−5425.

(18) Johansen, K. T.; Wubshet, S. G.; Nyberg, N. T.; Jaroszewski, J. W. From Retrospective Assessment to Prospective Decisions in Natural Product Isolation: HPLC-SPE-NMR Analysis of Carthamus Oxyacantha. *J. Nat. Prod.* **2011**, *74*, 2454−2461.

(19) Romero-González, R.; Vidal, J. L. M.; Aguilera-Luiz, M. M.; Frenich, A. G. Application of Conventional Solid-Phase Extraction for Multimycotoxin Analysis in Beers by Ultrahigh-Performance Liquid Chromatography-Tandem Mass Spectrometry. *J. Agric. Food Chem.* **2009**, *57*, 9385−9392.

(20) Basheer, C.; Alnedhary, A. A.; Rao, B. S. M.; Valliyaveettil, S.; Lee, H. K. Develepment and Application of Porous Membrane-Protected Carbon Nanotube Micro-solid Phase Extraction Combined with Gas Chromatography/Mass Spectrometry. *Anal. Chem.* **2006**, *78*, 2853−2858.

(21) Zhang, H.; Low, W. P.; Lee, H. K. Evaluation of Sulfonated Graphene Sheets as Sorbent for Micro-Solid-Phase Extraction Combined with Gas Chromatography-Mass Spectrometry. *J. Chromatogr. A* **2012**, *1233*, 16−21.

(22) Ge, D.; Lee, H. K. Water Stability of Zeolite Imidazolate Framework 8 and Application to Porous Membrane-Protected Micro-Solid-Phase Extraction of Polycyclic Aromatic Hydrocarbons from Environmental Water Samples. *J. Chromatogr. A* **2011**, *1218*, 8490−8495.

(23) Huang, Y. R.; Zhou, Q. X.; Xie, G. H. Development of Micro-Solid Phase Extraction with Titanate nanotube Array Modified by Cetyltrimethylammonium Bromide for Sensitive Determination of polycyclic Aromatic Hydrocarbons from Environmental Water Samples. *J. Hazard. Mater.* **2011**, *193*, 82−89.

(24) Bai, L.; Mei, B.; Guo, Q. Z.; Shi, Z. G.; Feng, Y. Q. Magnetic Solid-Phase Extraction of Hydrophyobic Analytes in Environmental



DOI: 10.1021/acsami.5b05241
*ACS Appl. Mater. Interfaces* 2015, 7, 22256−22263

Samples by a Surface Hydrophilic Carbon-Ferromagnetic Nanocomposite. *J. Chromatogr. A* **2010**, *1217*, 7331−7336.
(25) Hu, Y. L.; Huang, Z. L.; Liao, J.; Li, G. K. Chemical Bonding Approach For Fabrication of Hybrid Magnetic Metal-Organic Framework-5: High Efficient Adsorbents For Magnetic Enrichment of Trace Analytes. *Anal. Chem.* **2013**, *85*, 6885−6893.
(26) Zhao, Q.; Wei, F.; Luo, Y. B.; Ding, J.; Xiao, N.; Feng, Y. Q. J. Rapid Magnetic Solid-Phase Extraction Based on Magnetic Multiwalled Carbon Nantubes For the Determination of Polycyclic Aromatic Hydrocarbons in Edible Oils. *J. Agric. Food Chem.* **2011**, *59*, 12794−12800.
(27) Du, W.; Fu, Q.; Zhao, G.; Huang, P.; Jiao, Y. Y.; Wu, H.; Luo, Z. M.; Chang, C. Dummy-template molecularly imprinted solid phase extraction for selective analysis of ractopamine in pork. *Food Chem.* **2013**, *139*, 24−30.
(28) Hu, B.; Wang, S. B.; Wang, K.; Zhang, M.; Yu, S. H. Microwave-Assisted Rapid Facile "Green" Synthesis of Uniform Silver Nanoparticles: Self-Assembly into Multilayered Films and Their Optical Properties. *J. Phys. Chem. C* **2008**, *112*, 11169−11174.
(29) Lee, Y. J.; Park, S.; Seo, J. G.; Yoon, J. R.; Yi, J.; Song, I. K. Nano-sized Metal-Doped Carbon Aerogel for Pseudo-Capacitive Supercapacitor. *Curr. Appl. Phys.* **2011**, *11*, 631−635.
(30) Yang, W. J.; Wu, D. C.; Fu, R. W. Effect of Surface Chemistry on the Adsorption of Basic Dyes on Carbon Aerogels. *Colloids Surf., A* **2008**, *312*, 118−124.
(31) Wu, J. H.; Li, X. S.; Zhao, Y.; Gao, Q.; Guo, L.; Feng, Y. Q. Titania Coated Magnetic Mesoporous Hollow Silica Microspheres: Fabrication and Application to Selective Enrichment of Phosphpeptides. *Chem. Commun.* **2010**, *46*, 9031−9033.
(32) Gao, Q.; Luo, D.; Bai, M.; Chen, Z. W.; Feng, Y. Q. Rapid Determination of Estrogens in Milk Samples Based on Magnetite Nanoparticles/Polypyrrole Magnetic Solid-Phase Extraction Coupled with Liquid Chromatography-Tandem Mass Spectrometric. *J. Agric. Food Chem.* **2011**, *59*, 8543−7336.
(33) Economou, A.; Botitsi, H.; Antoniou, S.; Tsipi, D. Determination of Multi-Class Pesticides in Wines by Solid-Phase Extraction and Liquid Chromatography-Tandem Mass Spectrometry. *J. Chromatogr. A* **2009**, *1216*, 5856−5867.
(34) Dong, S. Y.; Huang, G. Q.; Hu, Q.; Shi, L.; Yao, Y. H.; Huang, T. L. Evaluation of IL-ATPS and IL-MAE for Simultaneous Determination of Herbicides and Plant Growth Regulators in Sediment. *Chromatographia* **2014**, *77*, 923−931.
(35) Dong, S. Y.; Huang, G. Q.; Lu, J. S.; Huang, T. L. Determination of fungicides in sediments using a dispersive liquid-liquid microextraction procedure based on solidification of floating organic drop. *J. Sep. Sci.* **2014**, *37*, 1337−1342.
(36) Yu, L. Z.; Wells, M. J. M. Establishing the Feasibility of Coupled Solid-Phase Extraction-Solid-Phase Derivatization for Acidic Herbicides. *J. Chromatogr. A* **2007**, *1143*, 16−25.
(37) Dong, S. Y.; Hu, Q.; Yang, Z.; Liu, R.; Huang, G. Q.; Huang, T. L. An Ionic Liquid-Based Ultrasound Assisted Dispersive Liquid-Liquid Microextraction Procedure Followed by HPLC for the Determination of Low Concentration of Phytocides in Soil. *Microchem. J.* **2013**, *110*, 221−226.
(38) Zhao, P. Y.; Wang, L.; Zhou, L.; Zhang, F. Z.; Kang, S.; Pan, C. P. Multi-walled carbon nanotubes as alternative reversed-dispersive solid phase extraction materials in pesticide multi-residue analysis with QuEChERS method. *J. Chromatogr. A* **2012**, *1225*, 17−25.


DOI: 10.1021/acsami.5b05241
*ACS Appl. Mater. Interfaces* 2015, 7, 22256−22263